The International Journal of Advanced Manufacturing Technology (2018) 97:1305–1314
https://doi.org/10.1007/s00170-018-1855-7

ORIGINAL ARTICLE

Numerical analysis of the influence of coatings on a cutting tool using COMSOL

Diego Corrêa Ferreira [1] · Elisan dos Santos Magalhães [1] · Rogério Fernandes Brito [2] · Sandro Metrevelle M. Lima E Silva [1]

Received: 27 September 2017 / Accepted: 6 March 2018 / Published online: 24 April 2018

Abstract
The determination of the thermal field in a turning process is fundamental to improve the process quality. Recently, the carbide tools have been coated with ceramic materials that present insulating characteristics. This work presents an analysis of the thermal effects of coating in a carbide tool during a turning process using the COMSOL® software and a nonlinear inverse problem. The thermal model consists of a coated carbide tool, a tool holder, and a shim represented by the transient three-dimensional heat diffusion equation with heat loss by convection and radiation. The heat flux, previously unknown, is obtained through the function specification method. In order to validate the methodology, the heat flux is compared with the author's previous work. Titanium nitride (TiN) and aluminum oxide (Al_2O_3) are utilized as the coating materials. Both coatings present the expected behavior when less heat is dissipated to the cutting tool substrate. The coated carbide tools present higher temperatures than the uncoated carbide tool in the contact area. The study also found that the thicker the coating, the higher the temperature in the contact area. The results presented in this work may help the development of new long-lasting coated carbide tools.

Keywords Inverse problems · Heat flux estimation · Cutting process · COMSOL · Coatings

1 Introduction

Reducing machining costs and the bad effects caused by using cooling lubricants are the main advantages of dry machining. However, modeling the process realistically is necessary to better understand the physical phenomena involved [1–3]. It is difficult to determine the temperature on the tool-chip interface due to the movement of the workpiece, chip obstruction and the small tool-chip contact area.

Experimental methods have their limitation to determine this temperature. In embedded thermocouple method, the position of the thermocouple close to the tool-chip contact area can interfere in the heat flux. Infrared measurement techniques also have their limitations, once it is not possible to measure the temperature directly due to chip obstruction on the rake face. Lately, numerical methods, like Finite Element method and Finite Difference method, have also been applied to simulate the tool-chip interface temperature. Nevertheless, without precisely knowing the heat flux at tool-chip interface, these methods cannot determine the cutting temperature directly [4]. Thus, inverse heat conduction techniques are a good alternative to obtain this temperature. These techniques allow the use of experimental data obtained from accessible regions [5, 6].

A comparison of the inverse techniques golden section, function specification, simulated annealing, and dynamic observers based on Green's function was proposed by Carvalho et al. [7]. An experimental methodology used these techniques

✉ Sandro Metrevelle M. Lima E Silva
metrevel@unifei.edu.br

Diego Corrêa Ferreira
diegoc.ferreira@unifei.edu.br

Elisan dos Santos Magalhães
elisan@unifei.edu.br

Rogério Fernandes Brito
rogbrito@unifei.edu.br

[1] Heat Transfer Laboratory, LabTC, Institute of Mechanical Engineering–IEM, Federal University of Itajubá, UNIFEI, Campus Prof José Rodrigues Seabra Av. BPS, 1303, Itajubá, MG 37500-903, Brazil

[2] Federal University of Itajubá, UNIFEI, Rua Irmã Ivone Drumond, 200 Distrito Industrial II, Itabira, MG 35903-087, Brazil

to determine the thermal fields and the heat generated in the tool-chip interface during a turning process. Liang et al. [8] proposed a quantitative investigation of temperature in the tool-chip interface during a machining process using a heat pipe as a heat exchanger to cool down a cutting tool. The finite difference method and an inverse procedure were used to determine the temperature. Similar work was also carried out by Liang et al. [4], where an inverse three-dimensional procedure was presented to investigate the tool-chip interface temperature in dry turning of the AISI 1045 steel. The temperature on the rake face of the cutting tool was measured by using an infrared thermography camera. These temperature values were later used to obtain the heat flux by the conjugate gradient method.

In order to better represent the thermal model in turning processes, Brito et al. [5] considered a more realistic geometry for the previous work of Brito et al. [9] and Carvalho et al. [10]. The function specification and the commercial software COMSOL® were used to estimate the heat flux and the temperature field in the contact area of a cutting tool.

The inverse heat conduction method has also been applied in the study of other machining processes. The amount of energy transferred to the workpiece during electric discharge machining (EDM) process was estimated using the Lavenberg-Marquardt method [11]. This inverse procedure facilitates the determination of the heat energy at discharge-workpiece interface in EDM processes, which yet is a challenge for existing numerical models.

The COMSOL® Multiphysics is finite element analysis software to solve physical problems with numerical models. For instance, the heat transfer in buildings was modeled in COMSOL® by Gerlich et al. [12]. Greiby et al. [13] joined MATLAB® and COMSOL® to estimate the nonlinear thermal conductivity of a cherry pomace. Suarez et al. [14] used COMSOL® to study the infrared photothermal radiometry of solids.

The present work is an improvement of the work developed by Brito et al. [5]. The main difference is that this work consists of nonlinear heat transfer by conduction, convection, and radiation in the COMSOL® model, differently from Brito et al. [5] who used CFX®. A new analysis of the maximum, minimum, and average temperatures in the contact area interface is also presented. A numerical code in MATLAB® in connection with COMSOL® is used to calculate the heat flux. Once the heat flux is known, COMSOL® is again used to solve the transient heat diffusion equation and obtain the temperature field in the model. The heat flux estimated in this work is compared with the heat flux of previous work to validate the methodology. The differences of the maximum temperature in the contact area between the coated and uncoated carbide tools of different coating thicknesses are also evaluated.

2 Methodology

2.1 The 3-D models

The 3-D thermal models consist of coated and uncoated carbide tools, an AISI 1045 steel tool holder, and a carbide shim. Figure 1 presents the fundamental dimensions of the models. These models were applied in the simulation in order to compare the thermal gradient when coated tools are used in the cutting process. The rake face, which is the region of the cutting tool in contact with the workpiece, is coated. The coating is a thin layer of a compound placed on the top surface of the substrate. The thermal contact between the coating and the substrate is considered perfect.

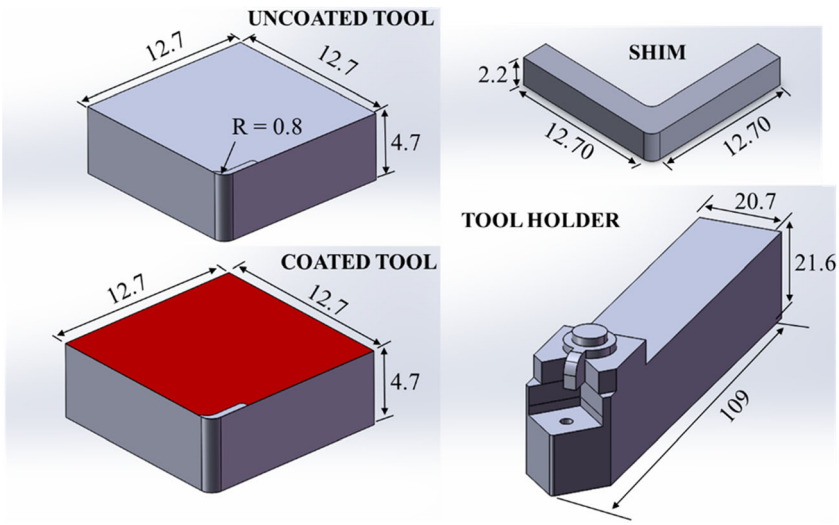

Fig. 1 Fundamental dimensions of the 3-D models in millimeter

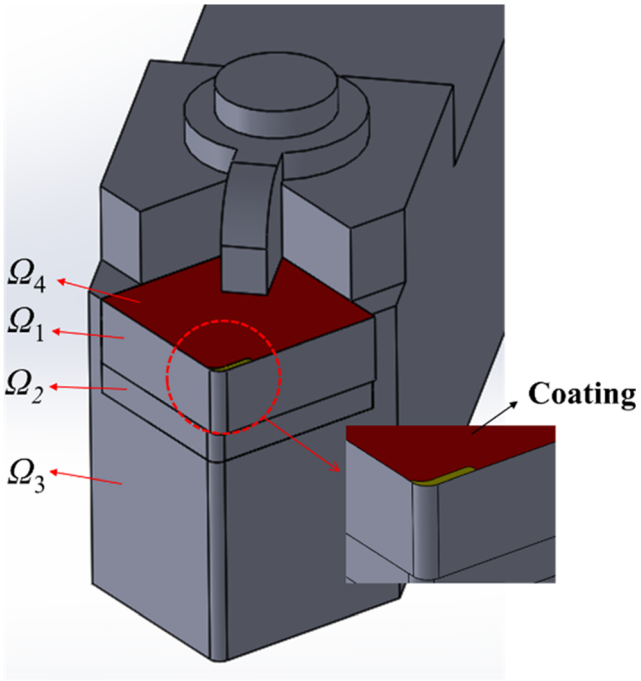

Fig. 2 All the domains of the model and the coating detail

To better exemplify, the models are divided into domains (Fig. 2): substrate of the carbide cutting tool (Ω_1), shim (Ω_2), tool holder (Ω_3), and coating (Ω_4). Each domain is divided into regions submitted to different boundary conditions like imposed heat flux, heat transfer by convection, radiation, and contact interface. Figure 3 presents the regions of the substrate domain of a coated tool and an uncoated tool.

Region S_1, highlighted in yellow, represents the contact area between the cutting tool and the workpiece, where the heat flux is applied during the cutting process. Region S_2 represents the entire cutting tool surface in contact with air and where the boundary conditions are natural convection and radiation. Region S_3 is the contact interface between the cutting tool and the tool holder. The model of the coated cutting tool (Fig. 3) is composed of the carbide substrate domain (Ω_1) and the coating domain (Ω_4). The regions on the coated cutting tool are the same as on the uncoated tool, except for S_4 which is coated. Region S_1 is the same for both models. This region was measured by Carvalho et al. [10] using an image system program with a video camera, Hitachi CCD, KP-110 model; a PC AMD K6 450 MHz; and GLOBAL LAB Image software. A comparison between the numerical contact area of this work and the work of Carvalho et al. [10] is presented in Fig. 4.

The friction on the flank face was not considered since artificially formed small land by honing or naturally, due to wear, was not observed [15]. Therefore, the heat distribution could be considered only on the normal rake face.

The tool holder domain (Ω_3) is also divided into two regions, once it receives part of the thermal energy from the cutting tool during the turning process. Region S_5 includes all the surfaces of the tool holder which are in contact with the shim and the cutting tool. The other surfaces comprehend region S_6, submitted to the boundary conditions of natural

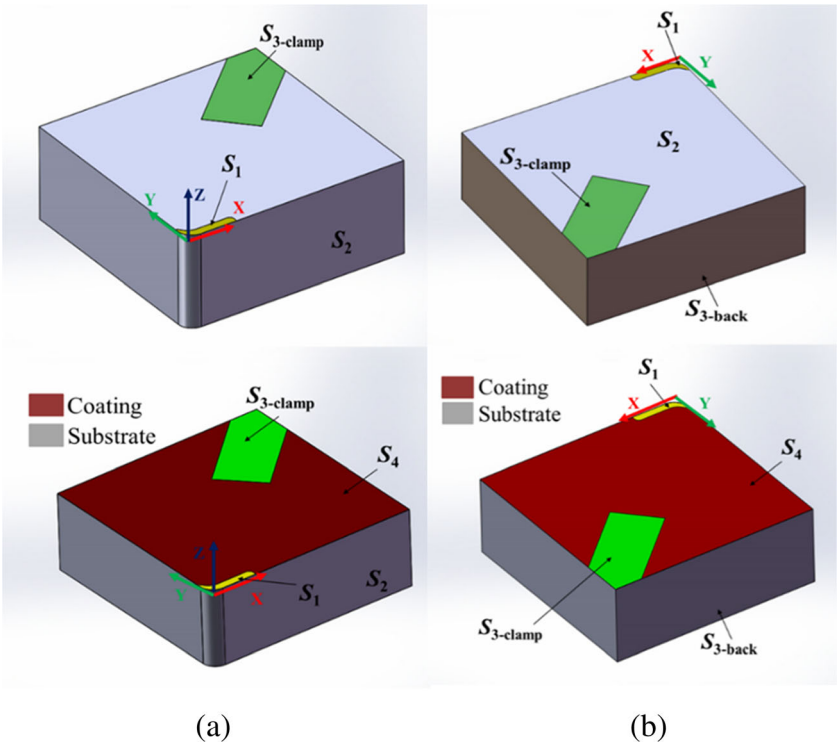

Fig. 3 Domain of the coated and uncoated cutting tools: (a) contact interface with the workpiece and (b) contact interface with the tool holder

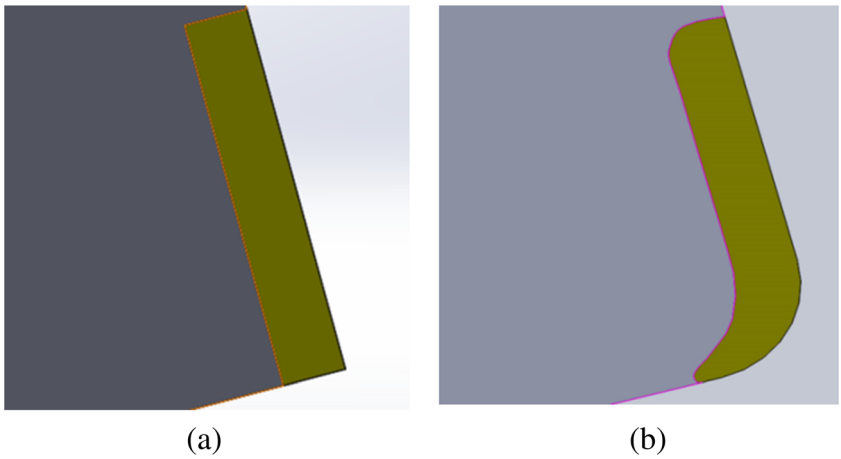

Fig. 4 Comparison of the numerical area in the computational model: (a) work by Carvalho et al. [10] and (b) present work

convection and radiation. The thermal contact between the carbide tool, shim, and tool holder was considered perfect. Figure 5 shows the regions of the tool holder.

2.2 Thermal properties

The thermal properties were considered nonlinear and built from fitting data found in literature; the emissivity values of the tool holder and the coating materials were considered constant. The thermal conductivity k (W/mK) and emissivity ε of the carbide material were taken from Jiang et al. [16], whereas the thermal diffusivity α (m/s^2) was taken from Grzesik et al. [17]. The thermal conductivity and emissivity for the coating materials and for the AISI 1045 steel were taken from Grzesik et al. [17]. The emissivity of the titanium nitride (TiN), aluminum oxide (Al_2O_3), and AISI 1045 steel were obtained from Yuste et al. [18], Wang et al. [19], and Polozine and Schaeffer [20], respectively. These values are shown in Table 1. Equations (1)–(9) present the fitted curves for the thermal properties in relation to the temperature (°C).

$$k_1(T) = 2.23 \times 10^{-8}T^3 - 2.22 \times 10^{-6}T^2 - 2.42 \times 10^{-2}T + 55.67 \quad 20 < T < 900 \tag{1}$$

$$k_2(T) = -3.31 \times 10^{-6}T^2 + 8.67 \times 10^{-3}T + 21.50 \quad 20 < T < 1200 \tag{2}$$

$$k_3(T) = 1.30 \times 10^{-5}T^2 - 2.65 \times 10^{-2}T + 19.10 \quad 20 < T < 1200 \tag{3}$$

$$k_4(T) = 4.87 \times 10^{-8}T^3 - 6.16 \times 10^{-5}T^2 - 1.66 \times 10^{-2}T + 38.60 \quad 20 < T < 1150 \tag{4}$$

$$\alpha_1(T) = -1.11 \times 10^{-14}T^3 + 3.11 \times 10^{-11}T^2 - 2.78 \times 10^{-8}T + 19.01 \times 10^{-6} \quad 20 < T < 1100 \tag{5}$$

$$\alpha_2(T) = 5.99 \times 10^{-11}T + 6.52 \times 10^{-6} \quad 20 < T < 1100 \tag{6}$$

$$\alpha_3(T) = -2.44 \times 10^{-14}T^3 + 4.07 \times 10^{-11}T^2 - 2.55 \times 10^{-8}T + 7.40 \times 10^{-6} \quad 20 < T < 700 \tag{7}$$

$$\alpha_4(T) = 2.00 \times 10^{-14}T^3 - 2.09 \times 10^{-11}T^2 - 7.62 \times 10^{-9}T + 12.80 \times 10^{-6} \quad 20 < T < 1150 \tag{8}$$

$$\varepsilon_1(T) = 5.06 \times 10^{-9}T^3 - 5.03 \times 10^{-6}T^2 + 2.31 \times 10^{-3}T - 4.12 \times 10^{-2} \quad 250 < T < 650 \tag{9}$$

where the subscript 1 is for the carbide, 2 for titanium nitride (TiN), 3 for aluminum oxide (Al_2O_3), and 4 for AISI 1045 steel.

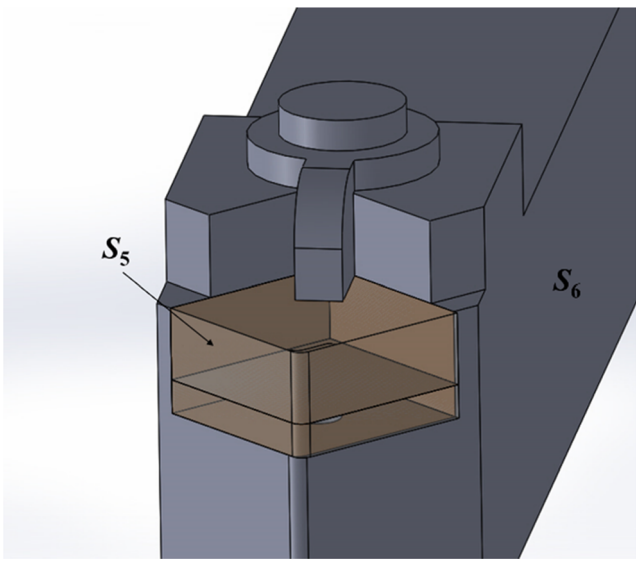

Fig. 5 Tool holder domain with the contact interfaces and the surfaces subjected to natural convection and radiation conditions

Table 1 Thermal emissivity for the coatings and the tool holder material

Material	TiN	Al_2O_3	AISI 1045
ε	0.2	0.85	0.83

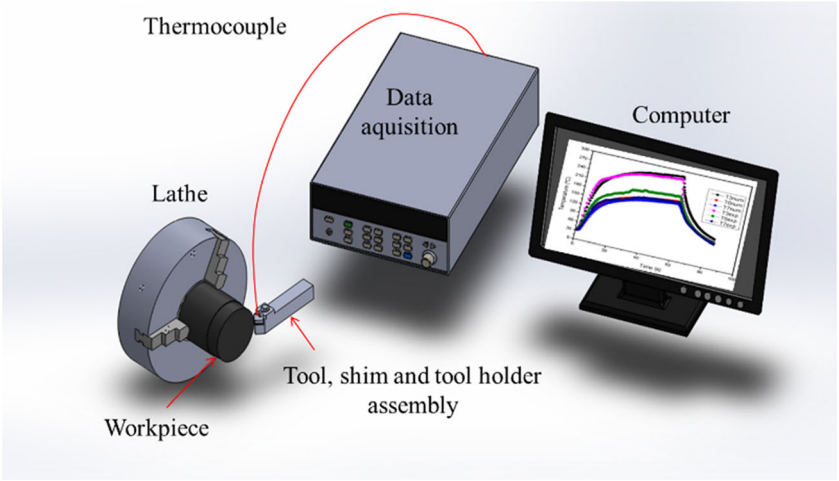

Fig. 6 Experimental apparatus used to acquire the temperature signals in the tool during turning

2.3 Direct thermal model

The thermal model may be described by the nonlinear transient three-dimensional diffusion equation:

$$\frac{\partial}{\partial x}\left(k(T)\frac{\partial T}{\partial x}\right)+\frac{\partial}{\partial y}\left(k(T)\frac{\partial T}{\partial y}\right)+\frac{\partial}{\partial z}\left(k(T)\frac{\partial T}{\partial z}\right) = \rho c(T)\frac{\partial T}{\partial t} \quad (10)$$

where x, y, and z are the Cartesian coordinates; t the physical time; T the temperature; k the thermal conductivity; c the specific heat; and ρ the density. Subject to the boundary conditions of convection and radiation:

$$-k(T)\frac{\partial T}{\partial \eta}(x,y,z,t) = h(T)(T-T_\infty)+\sigma\varepsilon(T)\left(T^4-T_\infty^4\right) \quad (11)$$

where k is the thermal conductivity, η the normal direction, h the heat transfer coefficient by convection, σ the Stefan-Boltzmann constant, ε the emissivity, and T_∞ the room temperature.

In the contact area, the boundary condition of the imposed heat flux q'' is applied:

$$-k(T)\frac{\partial T}{\partial z}(x,y,0,t) = q'' \quad (12)$$

The initial condition of the room temperature is used for the entire domain as follows:

$$T(x,y,z,0) = T_\infty \quad (13)$$

The solution of the previous equations is obtained with the use of the finite element method, through the commercial software COMSOL® *Multiphysics* 5.2. Due to the temperature gradients in the air and the gravitational field, there is an induction of natural convection currents around the assembly. In order to model the natural convection coefficient, which depends on the temperature, the software uses the empirical correlations from Bergman et al. [21].

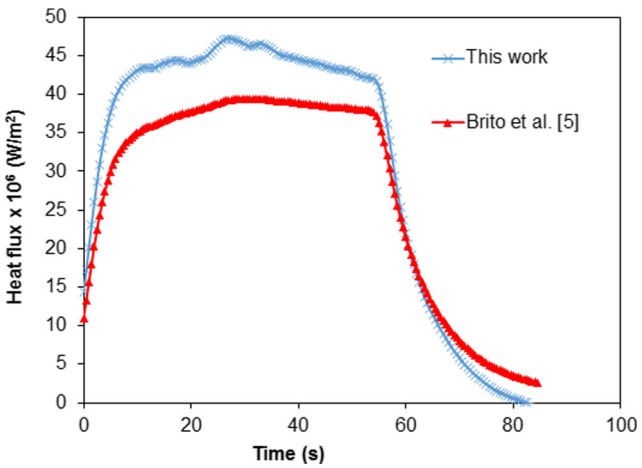

Fig. 7 A comparison of the estimated heat flux of this work and Brito et al. [4]

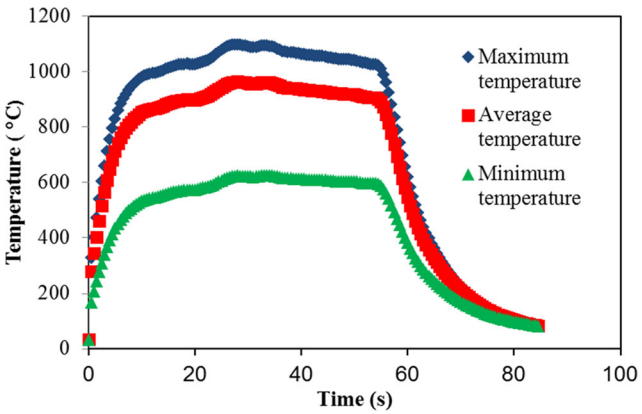

Fig. 8 Maximum, average, and minimum temperatures in the contact area

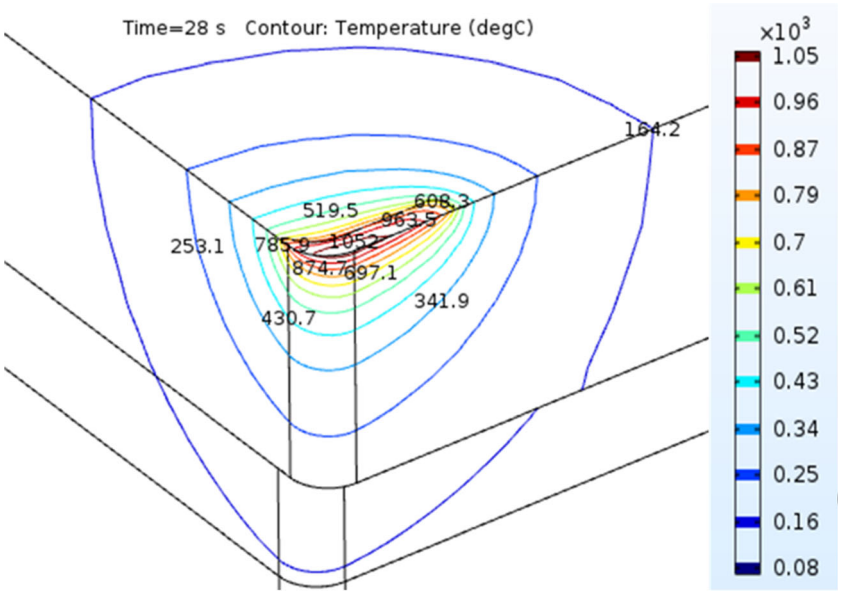

Fig. 9 Isothermal temperature lines in the region near the contact area

2.4 Inverse thermal model

The inverse technique adopted in this work is the function specification. In this technique, a determined value of future time steps r is used to estimate the heat flux at the present instant [22]. In the resolution of the inverse problem, the function specification searches for a heat flux value that minimizes the objective function given in Eq. (14), for each time step. A MATLAB program with the software COMSOL® *Multiphysics* 5.2 was used to estimate the heat flux.

$$F = \sum_{i=1}^{nt} \sum_{j=1}^{ns} \left(Y_{ij} - T_{ij}\right)^2 \tag{14}$$

where F is the objective function, i is the index to measure time, nt represents the total time of temperature measurements, j is the counter for the number of sensors, and ns represents the number of temperature sensors.

3 Experimental procedure

One of the major problems in the thermal analysis of a turning process is to accurately know the heat flux at the tool-chip interface. This work uses the experimental temperature data obtained by Carvalho et al. [10] to estimate the heat flux. The machining test was carried out in a conventional lathe IMOR MAXI-II-520-6CV without coolant. The material used in the experimental test was a cylindrical gray cast iron bar FC 20EB 126 ABNT of 77 mm in external diameter. The insert and tool holder used were cemented ISO SNUN12040408 K20/ Brassinter and ISO CSBNR 20K12/SANDVIK COROMAT,

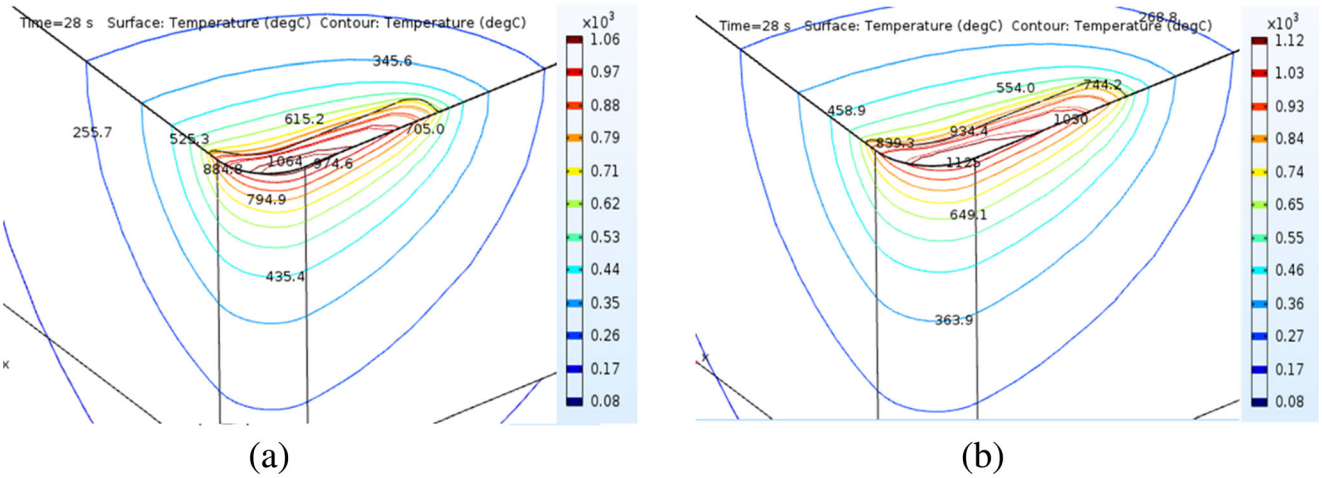

Fig. 10 Isothermal temperature lines in the region near the contact area: (a) TiN and (b) Al_2O_3

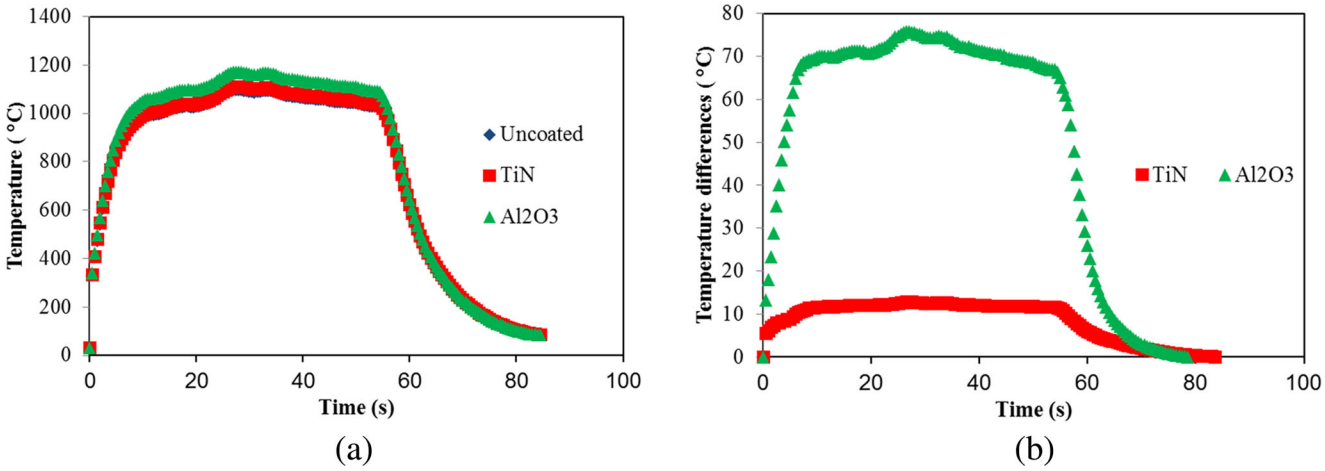

Fig. 11 **a** Maximum temperatures in the contact area of the uncoated and coated tools and **b** temperature differences between the coated and uncoated tools

respectively. The temperatures were measured on accessible locations of the insert, the shim, and the tool holder by using type K thermocouples (30 AWG) connected to a data acquisition system HP 75000 Series B controlled by a PC (Fig. 6). The location of the thermocouples used in the simulations and the cutting conditions to obtain the temperature data was according to the work of Brito et al. [5].

One of the improvements of this work is how the contact interface area is modeled. This numerical contact area had a shape closer to the real contact area (Fig. 5), while the numerical area used by Carvalho et al. [10] had a rectangular shape.

4 Result analysis

4.1 Heat flux

Once the experimental temperature values are known, the heat flux in the contact area can be calculated by minimizing the objective function (Eq. 14). Figure 7 presents the results of the heat flux obtained in this work and also compares with the heat flux results from Brito et al. [7]. Despite the fact of being the same physical problem, there are some differences between the heat flux values for each work. Brito et al. [5] made some geometric simplifications like using a solid shim instead of an L-shaped shim. Therefore, the authors did not take into account the variation of the heat transfer coefficient by convection and radiation in the numerical model. When this nonlinearity is accounted, a higher estimated heat flux is expected due to a greater heat loss by convection and radiation.

4.2 Uncoated carbide tool

The temperature profile can be achieved by knowing the heat flux value in the contact area between the workpiece and the cutting tool. The first simulation was carried out considering an uncoated carbide tool. A numerical probe was placed in the contact area (Fig. 5) in order to obtain the temperature in this region. The maximum, the average, and the minimum temperature values can be calculated with COMSOL® software (Fig. 8). High variations of the temperature values can be observed in this figure, even with the small contact area (1.43 mm^2). The maximum temperature reached was around 1097 °C, the average temperature reached was around 963 °C, and the minimum temperature was also around 626 °C. Figure 9 shows the isothermal temperature lines in the region near the contact area at instant $t = 28$ s.

4.3 Coated carbide tools

The simulation described in Section 4.2 is repeated, but now considering the coating which is represented by a thin 10-μm-thick layer. Figure 10 presents the isothermal temperature lines in the region near the contact area on the coated tool of TiN and Al_2O_3 at instant $t = 28$ s.

By analyzing Figs. 9 and 10, it may be noticed that the temperature in the contact area is higher on the coated tool than the uncoated tool. In order to better understand these results, Fig. 11a presents the maximum temperature in this

Table 2 Differences of the maximum temperatures in the contact area between the coated and uncoated tools for different coating thicknesses

Coating thickness (μm)	TiN (°C)	Al_2O_3 (°C)
10	12.7	75.5
20	25.2	151.5
50	61.1	351.8
100	117.1	663.5

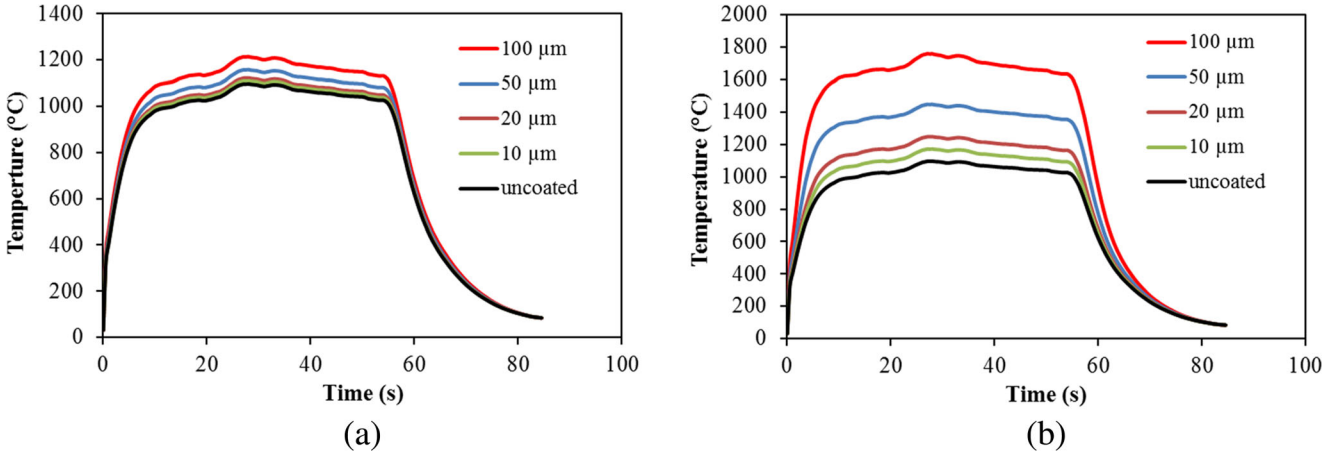

Fig. 12 Maximum temperature curve in the contact area for different coating thickness values: (a) TiN and (b) Al_2O_3

region at instant $t = 28$ s, on the uncoated tool, the TiN-coated tool, and the Al_2O_3-coated tool. Figure 11b shows the temperature differences between the coated tools and the uncoated tool.

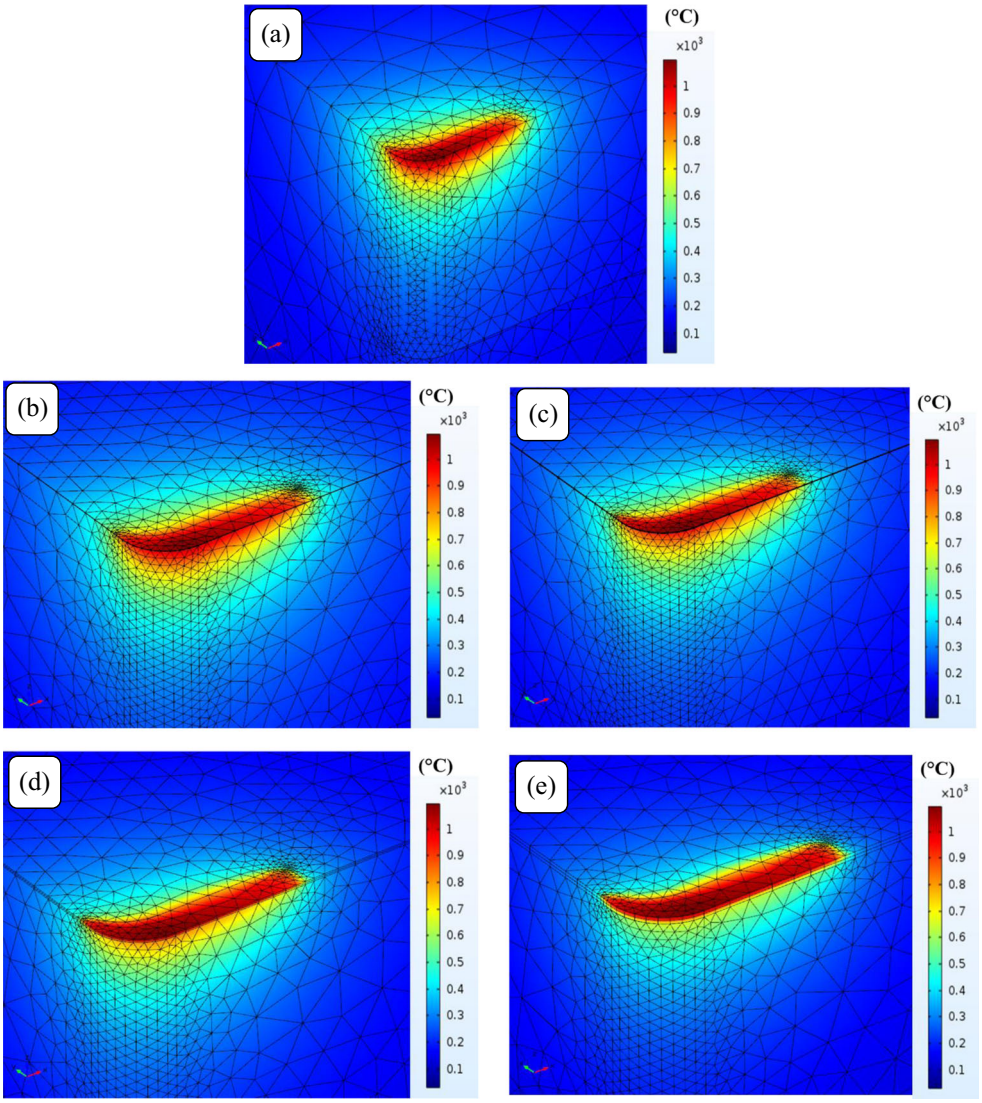

Fig. 13 Influence of the Al_2O_3 coating thickness in the cutting tool temperature field: **a** uncoated tool, **b** 10 µm, **c** 20 µm, **d** 50 µm, and **e** 100 µm

It may be verified in Fig. 11a that the curves of maximum temperature of the coated and uncoated tools have the same behavior. The maximum temperature curve of the TiN-coated tool overlaps the maximum temperature curve of the uncoated tool, not presenting a relevant temperature difference. This fact may be noticed in Fig. 11b at instant $t = 28$ s. The maximum temperature difference between the TiN-coated tool and the uncoated tool is around 12.7 °C. For the Al_2O_3-coated tool, the maximum temperature curve is above the maximum temperature curve of the uncoated tool, as may be seen in Fig. 11a. In Fig. 11b, at instant $t = 28$ s, the maximum difference of temperature between the Al_2O_3-coated tool and the uncoated tool is around 75.5 °C. In the work of Brito et al. [9], the maximum temperature difference obtained was around 8.2 °C using the same 10-μm-thick coated carbide tool.

By observing the previous figures, one may conclude that the coating retains the heat on the top face of the cutting tool, not letting the heat penetrate the cutting tool substrate and thus increasing the cutting tool lifespan. The Al_2O_3 coating presents better insulating characteristic than the TiN since it has a lower thermal conductivity value.

4.4 Influence of the coating thickness

As previously shown, the coatings used in the cutting tools have insulating characteristics and play the role of protecting the substrate of the cutting tool with respect to heat. To further evidence this effect, the simulations of Section 4.3 are repeated considering thicker coatings: 20, 50, and 100 μm (Table 2 and Fig. 12).

When the coating thickness value of both materials is increased, the maximum temperature in the contact area also increases (Fig. 12). Table 2 also shows this fact where the maximum temperature difference in the contact area between the coated tool and the uncoated tool for different coating thickness values may be seen. Figure 13 presents the temperature field near the contact interface area for the uncoated tool and the Al_2O_3-coated tool for different coating thicknesses at the instant of $t = 28$ s. This figure shows the heat behavior when the coating thickness increases.

In Fig. 13a, which represents the uncoated tool, it may be noticed that the heat deeply penetrates the cutting tool substrate and consequently, the temperature field is large. When using the coating on the cutting tool (Fig. 13b), the temperature field begins decreasing slightly. By increasing the coating thickness (Fig. 13c–e), the temperature field decreases even more, which may be noticed from the red color in the figures. Thus, the coating holds the heat on the upper face of the cutting tool and does not spread it to the cutting tool substrate which would be harmful for the cutting tool lifespan.

5 Conclusions

This work presented the coating effect on the temperature field of the cemented carbide cutting tool. The coating effect was observed by comparing the temperature between the uncoated and coated materials.

The following conclusions may be cited regarding the numerical results obtained for the thermal model of heat transfer in coated cutting tools:

(1) The coating thickness was numerically increased to highlight the coating influence on the cemented carbide cutting tool. Despite the small contact area, the coated and uncoated carbide cutting tools presented a peak difference in the cutting region of 12.7 °C for the TiN and 75.5 °C for the Al_2O_3.
(2) The 10-μm-thick coated tool models presented the expected behavior, once the maximum temperature in the contact area was higher when compared to the maximum temperature on the contact area of the uncoated tool.
(3) By increasing the coating thickness, the maximum temperature in the contact area also increases.
(4) The best results were obtained using the Al_2O_3 coating, once it has a thermal conductivity value lower than the thermal conductivity value of the TiN coating. Thus, the coating fulfills its role of protecting the substrate of the cutting tool with respect to heat.

Acknowledgements The authors would like to thank CNPq, CAPES, and FAPEMIG for their financial support.

References

1. Deppermann M, Kneer R (2015) Determination of the heat flux to the workpiece during dry turning by inverse methods. Prod Eng 9: 465–471. https://doi.org/10.1007/s11740-015-0635-6
2. Lazard M, Remy B (2008) Heat flux and temperature estimation during cutting process through regularization technique. In: 5th European Thermal-Sciences Conference. Eindhoven, The Netherlands
3. Ingraci Neto RR, Scalon VL, Fiocchi AA, Sanchez LEA (2016) Indirect cooling of the cutting tool with a pumped two-phase system in turning of AISI 1045 steel. Int J Adv Manuf Technol 87:2485–2495. https://doi.org/10.1007/s00170-016-8620-6
4. Liang L, Xu H, Ke Z (2013) An improved three-dimensional inverse heat conduction procedure to determine the tool-chip interface temperature in dry turning. Int J Therm Sci 64:152–161. https://doi.org/10.1016/j.ijthermalsci.2012.08.012
5. Brito RF, Carvalho SR, Lima E, Silva SMM (2015) Experimental investigation of thermal aspects in a cutting tool using comsol and inverse problem. Appl Therm Eng 86:60–68. https://doi.org/10.1016/j.applthermaleng.2015.03.083
6. Munoz-Sánchez A, González-Farias IM, Soldani X, Miguélez MH (2011) Hybrid FE/ANN and LPR approach for the inverse identification of material parameters from cutting tests. Int J Adv Manuf Technol 54:21–33. https://doi.org/10.1007/s00170-010-2922-x

7. De Carvalho SR, Dos Santos MR, De Souza PFB et al (2009) Comparison of inverse methods in the determination of heat flux and temperature in cutting tool during a machining process. High Temp-High Press 38:5–9
8. Liang L, Quan Y (2013) Investigation of heat partition in dry turning assisted by heat pipe cooling. Int J Adv Manuf Technol 66: 1931–1941. https://doi.org/10.1007/s00170-012-4471-y
9. Brito RF, de Carvalho SR, de Lima E Silva SMM, Ferreira JR (2009) Thermal analysis in coated cutting tools. Int Commun Heat Mass Transf 36:314–321. https://doi.org/10.1016/j.icheatmasstransfer.2009.01.009
10. Carvalho SR, Lima e Silva SMM, Machado AR, Guimarães G (2006) Temperature determination at the chip-tool interface using an inverse thermal model considering the tool and tool holder. J Mater Process Technol 179:97–104. https://doi.org/10.1016/j.jmatprotec.2006.03.086
11. Shabgard M, Akhbari S (2016) An inverse heat conduction method to determine the energy transferred to the workpiece in EDM process. Int J Adv Manuf Technol 83:1037–1045. https://doi.org/10.1007/s00170-015-7651-8
12. Gerlich V, Sulovská K, Zálešák M (2013) COMSOL Multiphysics validation as simulation software for heat transfer calculation in buildings: building simulation software validation. Meas J Int Meas Confed 46:2003–2012. https://doi.org/10.1016/j.measurement.2013.02.020
13. Greiby I, Mishra DK, Dolan KD (2014) Inverse method to sequentially estimate temperature-dependent thermal conductivity of cherry pomace during nonisothermal heating. J Food Eng 127:16–23. https://doi.org/10.1016/j.jfoodeng.2013.10.039
14. Suarez V, Hernández Wong J, Nogal U, Calderón A, Rojas-Trigos JB, Juárez AG, Marín E (2014) Study of the heat transfer in solids using infrared photothermal radiometry and simulation by COMSOL Multiphysics. Appl Radiat Isot 83:260–263. https://doi.org/10.1016/j.apradiso.2013.04.010
15. Grzesik W, Rech J, Zak K (2014) Determination of friction in metal cutting with tool wear and flank face effects. Wear 317:8–16. https://doi.org/10.1016/j.wear.2014.05.003
16. Jiang F, Zhang T, Yan L (2016) Estimation of temperature-dependent heat transfer coefficients in near-dry cutting. Int J Adv Manuf Technol 86:1207–1218. https://doi.org/10.1007/s00170-015-8293-6
17. Grzesik W, Niesłony P, Bartoszuk M (2009) Modelling of the cutting process analytical and simulation methods. Adv Manuf Sci Technol 33:5–29
18. Yuste M, Galindo RE, Sánchez O, Cano D, Casasola R, Albella JM (2010) Correlation between structure and optical properties in low emissivity coatings for solar thermal collectors. In: Thin Solid Films pp 5720–5723, 518 https://doi.org/10.1016/j.tsf.2010.05.056
19. Wang J, Song B, Zhang X, Song Y, Wu G (2011) Simultaneous measurements of thermal properties of individual carbon fibers. Int J Thermophys 32:974–983. https://doi.org/10.1007/s10765-011-0961-7
20. Polozine A, Schaeffer L (2005) Exact and approximate methods for determining the thermal parameters of the forging process. J Mater Process Technol 170:611–615. https://doi.org/10.1016/j.jmatprotec.2005.06.041
21. Bergman TL, Lavine AS, Incropera FP, DeWitt DP (2011) Fundamentals of heat and mass transfer, 7th ed. Wiley, New York
22. Beck JV, Blackwell B, St Clair, CR Jr (1985) Inverse heat conduction: ill-posed problems, John Wiley and Sons, New York